Sensitivity Analysis of Ground Impedance on Horizontal Full-Scale Rocket Motor Test Fire

Samuel Hord

A senior thesis submitted to the faculty of

Brigham Young University

In partial fulfillment of the requirements for the degree of

Bachelor of Science

Dr. Tracianne B. Neilsen, Advisor

Dr. Kent L. Gee, Co-advisor

Department of Physics and Astronomy

Brigham Young University

April 2015

ABSTRACT

Sensitivity Analysis of Ground Impedance on Horizontal Full-Scale Rocket Motor Test Fire

Samuel Hord

Department of Physics and Astronomy

Bachelor of Science

Ground reflections have a significant impact on the propagation of sound from a rocket firing. The impedance of the ground relies strongly on effective flow resistivity of the surface and determines the frequencies at which interference nulls occur. A softer ground, with lower effective flow resistivity, shifts the location of interference nulls to lower frequencies than expected for a harder ground. The difference in the spectral shapes from horizontal firings of GEM-60 rocket motors, over snowy and hard ground, clearly shows this effect and has been modeled. Different flow resistivity values yield reasonable comparisons to the results of horizontal GEM-60 test firings. A sensitivity analysis was performed to develop a method for obtaining reasonable flow resistivity values, with the results comparable to those supplied by the current literature.

Table of Contents

LIST OF FIGURES

Chapter 1

Introduction

Communications satellites, telescopes in space, rovers on Mars, the international space station—clearly, rockets are an important element of the information age. Studying the acoustics of rocket motors yields knowledge and understanding that will better enable scientists to protect investments in vehicles, payloads, and launch pads. The effects of ground reflections are important factors in studying the propagation of sound from a rocket motor[1].

Shock and vibration can destroy launch pads and prevent satellites and launch vehicles from fulfilling their missions, which is why it is important to understand the effects of ground reflections. Understanding the effect of ground reflections will help us better characterize the near-launch pad acoustical environment. In addition, there is much that we can learn about the source of sound energy emanating from a rocket motor by studying data collected from horizontal rocket motor firings. Since this data must by necessity be collected in a half-space, the ground reflections play a critical role in understanding and interpreting the data.

An important consideration to take into account when studying rocket noise is the interference caused by ground reflections. Sound emanated from the rocket motor will reach field microphones by both direct and reflected paths[2]. This will result in constructive and destructive interference. Such interference causes misleading information to be recorded by our microphones. Interference caused by path length difference is not unique to acoustics: for example, differences in geometry account for patterns of interference in single- and double-slit optical experiments. Sound waves traveling through air, however, undergo some additional significant interactions. The geometry, the acoustic properties of the ground, the turbulence caused by the amplitude of the source and the ambient conditions—all these play a significant role in the propagation of sound in an outdoor environment.

The purpose of this study is to provide an analysis of the relative importance of these various factors as they relate to horizontal rocket motor test fires. How important are the characteristics of the ground relative to the geometries of the experimental set up? What changes in geometry have the most impact on the results obtained? How do uncertainties in the geometry of the set up relate to uncertainties in the parameters chosen to characterize the ground? The answers to these questions can assist in developing better models to predict the effects of turbulence and ground reflections, and help us to better understand the nature of the acoustics at play during rocket motor firings.

1.1 Background

Ground reflections have been studied extensively[3]. Although the single parameter model developed by Delaney and Bazley[4] does not apply in every situation, it is useful for quick, easy measurements of the acoustic impedance of the ground. This paper uses the single parameter

method to study the effect of snow-covered ground on the signal received by a transducer in the far field.

1.2 Ground Reflections

The method of images can be used to compute the effect that path length differences have on propagating sound waves[5]. In Figure 3, sound emanating from a source S reaches a receiver R by a direct path (r_d) and by a reflected path (r_r). The length of r_r can be shown by reflecting the source across the line designating the ground surface to create an image source (S_i). This reflected path makes an angle φ with the horizontal.

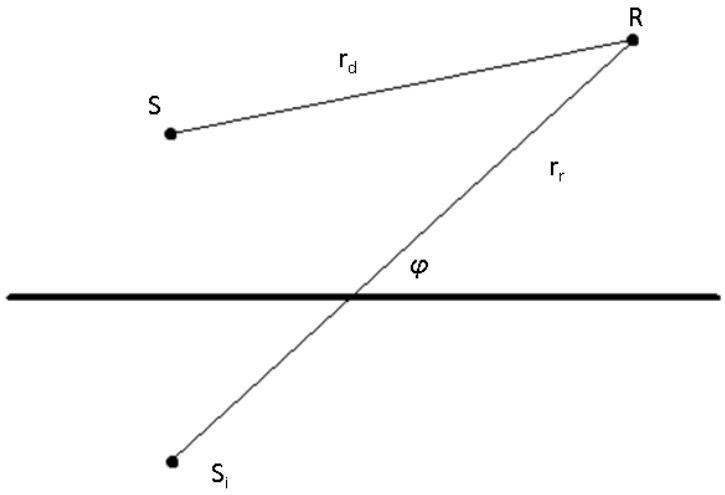

Figure 1 Direct and reflected paths from a source to a receiver

The received pressure is given by Equation [1][6] from Daigle's article "Effects of atmospheric turbulence on the interference of sound waves above a finite impedance boundary":

$$p = \frac{A_d}{r_d}\exp[i(k_d r_d - \omega t)] + Q\frac{A_r}{r_r}\exp[i(k_r r_r - \omega t)]$$

The pressure arriving at the receiver can be expressed as the sum of waves incident from two simple sources: the real source and an image source. The amplitude of each wave is

inversely proportional to the distance from its source. The theory has been well-developed[3,7] and will only be summarized here. Pressure from the image source is multiplied by a strength factor *Q*, due to the effect of the ground reflection. The image source strength *Q* is related to the amplitude of the incident pressure wave by the complex reflection coefficient R_p, which is given by Equation [2] in the aforementioned article by Daigle[7]:

$$R_p = \frac{[Z_2 \sin\phi - Z_1(1 - k_1^2/k_2^2 \cos^2\phi)^{1/2}]}{[Z_2 \sin\phi + Z_1(1 - k_1^2/k_2^2 \cos^2\phi)^{\frac{1}{2}}]}$$

The complex reflection coefficient R_p is determined by the acoustic impedances and wave numbers of both the air and the ground. The acoustic impedance and wave number of the ground, Z_2 and k_2, are complex quantities that can be determined empirically by the following relationships:

$$Z_2 = R_2 + iX_2$$

$$k_2 = \alpha_2 + i\beta_2$$

$$R_2/\rho_1 c_1 = 1 + 9.08(f/\sigma)^{-0.75}$$

$$X_2/\rho_1 c_1 = +11.9(f/\sigma)^{-0.73}$$

$$\alpha_2/k_1 = 1 + 10.8\,(f/\sigma)^{-0.70}$$

$$\beta_2/k_1 = 10.3(f/\sigma)^{-0.59}$$

These equations come from Equations [5]-[8][3] in the 1983 article by Embleton titled "Effective flow resistivity of ground surfaces determined by acoustical measurement." The real and complex components of the ground impedance and wave number depend on the value of sigma (σ), the effective flow resistivity of the ground[4].

1.3 Finite Impedance

The sigma value associated with the ground is limited by thermal-conduction at a viscous boundary layer[3]. Figure 2 shows the relative sound pressure level (SPL) in decibels as a function of frequency for several different sigma values. At low frequencies, ground reflections result in a pressure doubling, which is shown in Figure 2 as a 6 dB increase in sound pressure level. This is expected in the case of two in-phase sources, meaning that the image source and the real source are perfectly correlated[1]. Higher values of effective flow resistivity yield primary interference nulls at higher frequencies, whereas lower sigma values have primary interference nulls at lower frequencies.

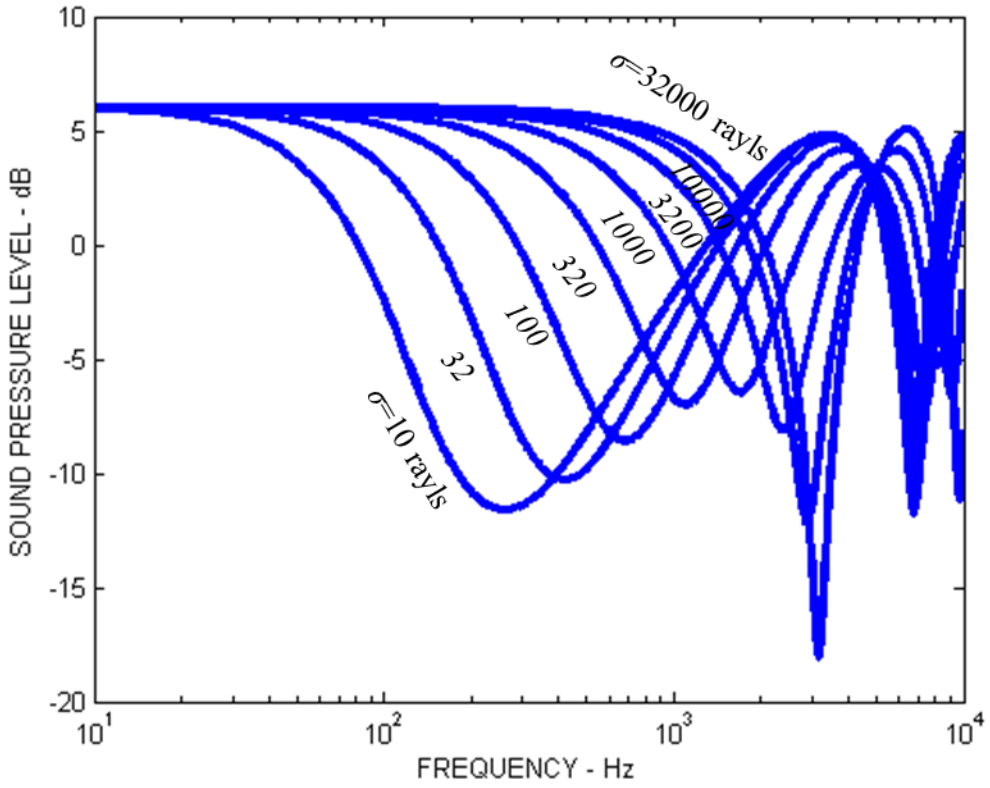

Figure 2 Relative sound pressure level as a function of frequency for several sigma values

1.4 Measuring ground impedance

Methods for measuring ground impedance are well-documented[8], and an example using the ANSI standard is found in Appendix A. Ideally, several measurements are made over a flat,

level ground surface[8]. Measuring ground impedance for a rocket test presents two unique challenges. The ground is not necessarily level, uniform, or smooth, and the height of the microphone relative to the source height is difficult to determine due to variations in the terrain. The size of the area of interest also presents a problem. Since measurements are taken in the far field, different receivers at different locations can experience different ground effects.

1.5 Effects of Turbulence

Figure 2 shows a repeating pattern of interference nulls; however, turbulence caused by wind and temperature variations reduces the depth of interference nulls at high frequencies. In fact, the power spectral density at the upper frequency range decays exponentially at upper frequencies. Therefore, the primary concern of this study is the first big interference null, which occurs between 100 and 1000 Hz, and which can be seen clearly in the rocket data[1].

Chapter 2

Full-scale Experimental Setup

Rocket motors present unique challenges in acoustics due to the shear volume of acoustic energy they emit. At such high amplitudes, many nonlinear assumptions fall apart[9]. There is a much to be learned about acoustics that would be impossible to glean from scaled-down experiments. Brigham Young University teamed up with Alliant Techsystems (ATK) in the summer of 2008 and winter of 2009 to take measurements during a pair of full-scale horizontal rocket motor tests. The data sets collected have been well-documented in several papers[1,9,10,11] and have lent valuable insight into high-energy acoustic phenomena.

2.1 GEM-60 Rocket Specifications

The sensitivity analysis draws on data collected during a full-scale rocket motor test fire performed at ATK near Brigham City, Utah, on February 19, 2009. The rocket motor was a GEM-60 (Graphite-Epoxy Motor) solid rocket booster, commonly used to increase the payload of Delta IV rockets[12]. This thirteen-meter-long rocket packs 879,000 Newtons of thrust. It allows

the Delta IV to carry an additional 2000-2500 kilograms into geosynchronous transfer orbit (GTO).

2.2 Experimental Setup

Various aspects of this experiment have been referenced in papers by Kent Gee, Traci Neilsen, Michael James, etc. [1,9,10,11] A single GEM-60 rocket motor was fired horizontally above the ground. Figure 3 shows the coordinate system used to designate the positions of the microphones used.

Of the large data sets, a select number of locations, at which there were mics in each experiment, are used in this work. Several 6.35 mm GRAS 40BD pressure microphones recorded the data presented in this paper from their field positions along the 50^0 and 60^0 radials (relative to the plume axis) at distances of 76, 105, and 305 m (250, 500, and 1000 ft) from the origin. The origin was about 10 m downstream from the nozzle[9,10], and represents the area of maximum sound radiation from the rocket motor.

2.3 Characteristics of the environment

As shown in Figure 3, the ground around the experiment was hard and rocky, with the occasional sage brush and rabbit hole. For the February test, this ground was covered by about 45 cm (18 inches) of snow. This non-ideal terrain complicates the propagation paths as the sound travels from the rocket plume to the microphones.

Figure 4 shows the power spectral density measured in February by the microphones along the 50^0 radial, as well as their overall sound pressure levels (OASPL). Sound arriving at any given microphone will experience constructive and destructive interference due to path length differences and due to the image source strength coefficient Q. This is manifest in the

main dip in pressure between 100 Hz and 200 Hz as shown in Figure 4. The overall sound pressure level at each microphone drops as distance from the source increases.

Hard ground is very reflective, which increases the frequency at which this destructive interference null occurs. The covering of snow, on the other hand, causes a phase shift in the reflected sound wave, resulting in a lower frequency of the main interference null. Although ground reflection models predict a repeating pattern of interference nulls at higher frequencies, these patterns are smeared out due to nonlinear atmospheric effects, such as wind and temperature gradients. Thus, the pressure appears to roll off linearly at frequencies above 700 Hz.

Since the mics are in the far field, the path length difference between direct and reflected sound waves is much more sensitive to changes in height (along the z axis) than to changes in range (along the r axis). The height of each microphone was estimated to be between one and two m off the ground, but the exact height relative to the plume was impossible to measure due to the terrain. The following chapter outlines a sensitivity analysis suitable for determining the effective flow resistivity given the uncertainty of the height of each microphone relative to the sound source.

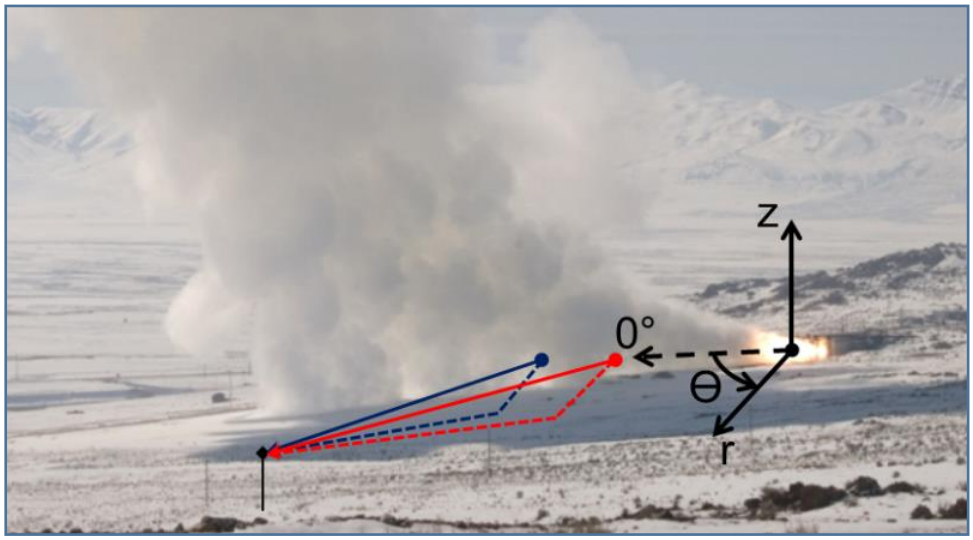

Figure 3 Full-scale Experimental Setup

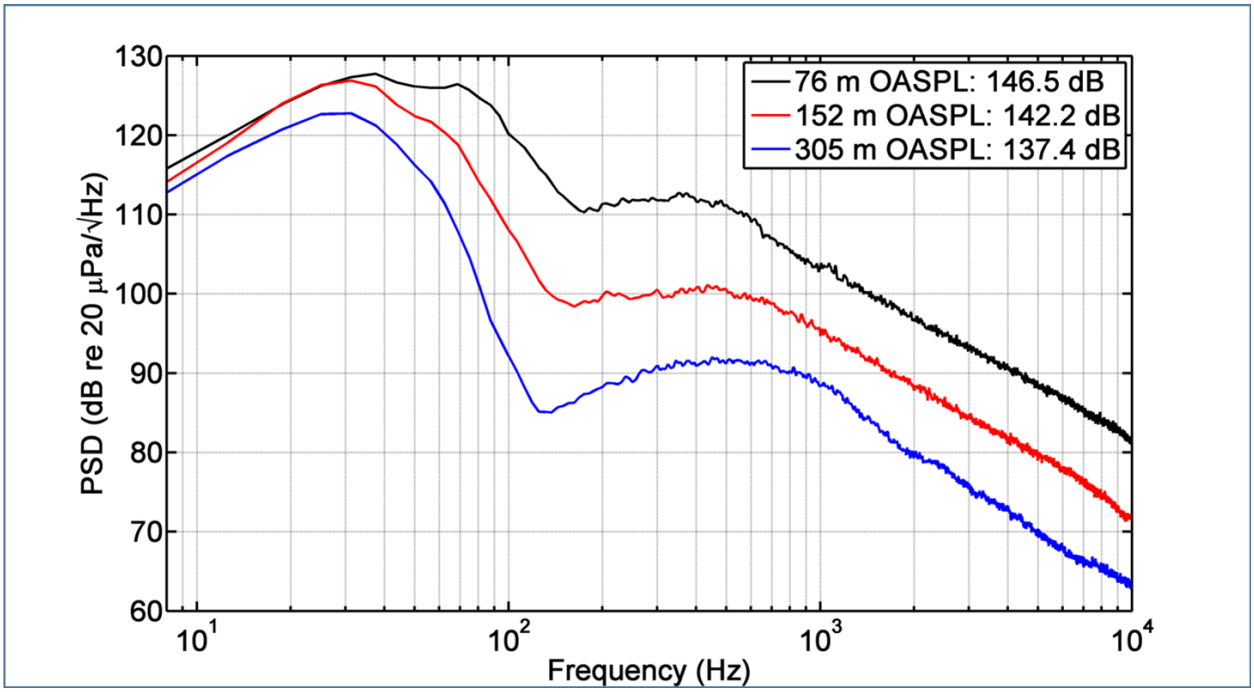

Figure 4 Power Spectral Density (PSD) along 50^0 radial

Chapter 3

Results and Conclusions

3.1 Measurement of interference nulls

Figure 3 shows the sound pressure level recorded by a microphone at 76 m along the 60^0 radial. The classic reflection model is shown in red for that geometry at a height of 1.5 m relative to the plume. The first major interference null of each curve is marked with a blue circle. The difference in frequency between the two nulls is indicated by Δf. The goal of this study is to discover parameters that will predict the frequency of the first interference null by minimizing Δf.

Figure 4 contains the same sound pressure curve as Figure 3, with three different z values chosen for the reflection model at a sigma value of 20,000 rayls. Figure 5 shows the results of those same geometries for a sigma value of 50,000 rayls. As indicated by these figures, the value of Δf is sensitive to both the effective flow resistivity chosen to characterize the ground and to the height of the receiver relative to the source.

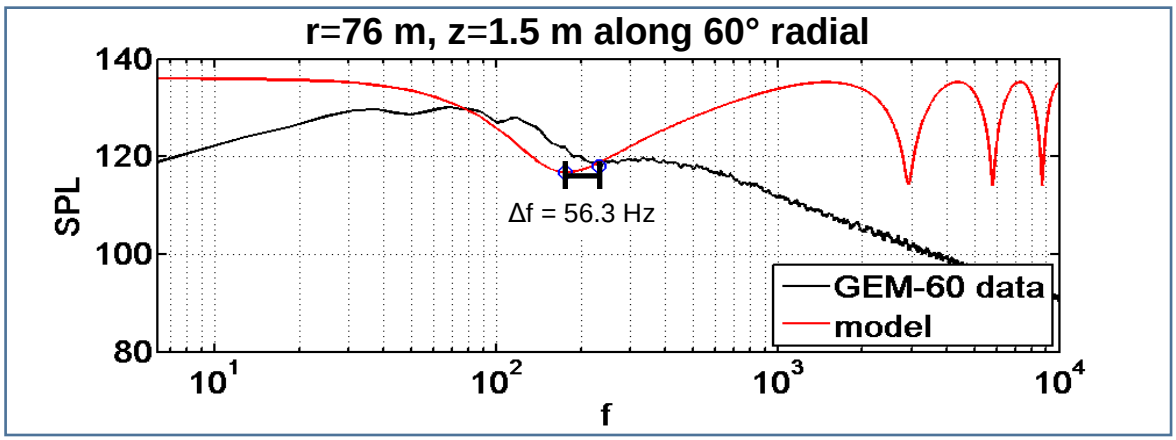

Figure 5 Sound Pressure Level with Ground Reflection Model

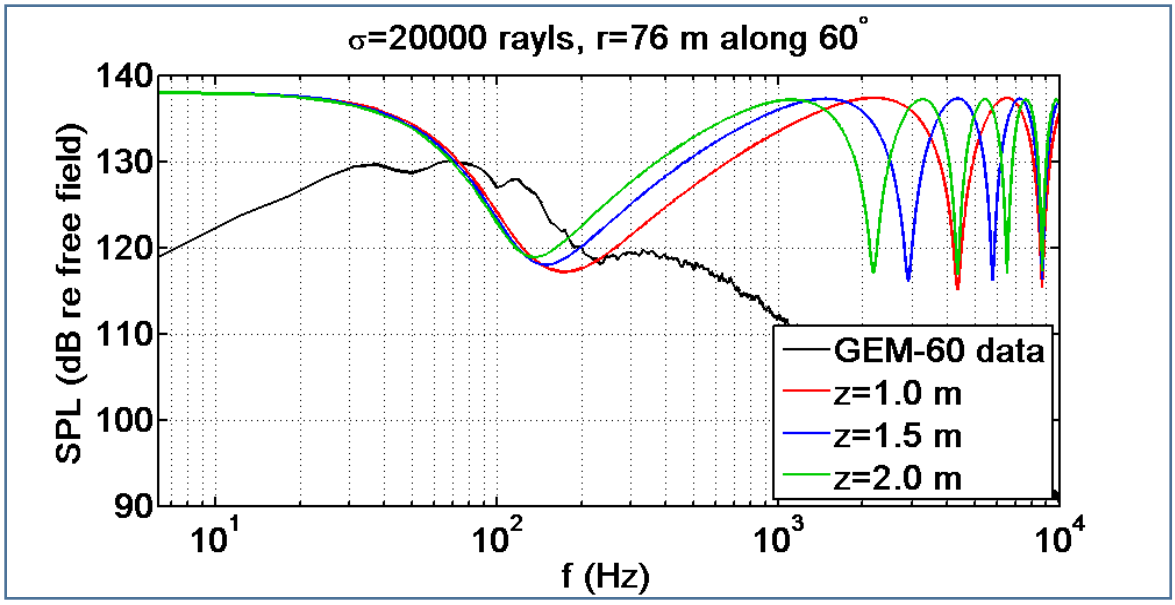

Figure 6 Ground reflection model with several different heights shown

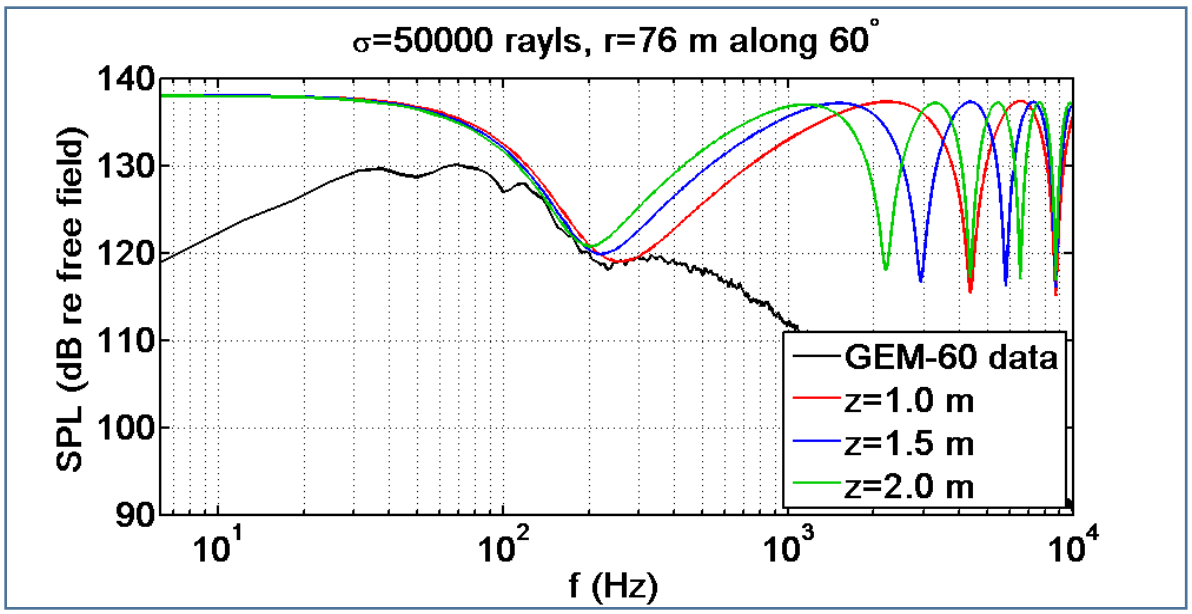

Figure 7 Ground reflection model with several different heights shown

3.2 Sensitivity Analysis

The goal of the sensitivity analysis is to determine a reasonable range of sigma values given the uncertainty in the microphone height with respect to the sound source. To accomplish this, the difference between the first local minimum of the ground reflection model and the low frequency dip in the GEM-60 data was found. I computed the curves for a wide range of heights and sigma values, found the first minima, and subtracted it from the frequency of the null from the rocket data. Then I plotted each combination of height and sigma value, with the magnitude of Δf depicted in color for each combination, as shown in Figures 6-9. The combinations that best match the frequency null of the data collected at each microphone location are shown in dark blue (smaller Δf), with greater differences in Δf shown in red. A white rectangle illustrates the sweet spot: between one to two m high and in a range of sigma values that leads to a very small Δf. Expected sigma values for snow-covered terrain range anywhere from twenty-five to fifty thousand rayls[1].

[1] Embleton. JASA 1983 (fix this format later)

3.3 Interpretation of Results

Figure 8 shows the sensitivity analysis plot for the microphone located 76 m along the 60^0 radial. The upper left quadrant of the white rectangle shows Δf values ranging from the thirties to upper forties. This indicates a combination of height and effective flow resistivity that is a poor match to the GEM-60 rocket data. The lower half of the white rectangle shows a much better agreement to the data; therefore, it is reasonable to assume that the microphone was 1½ -2 m above the sound source. The range of sigma values from forty to sixty thousand rayls is towards the upper end of the values recorded by Embleton.[3]

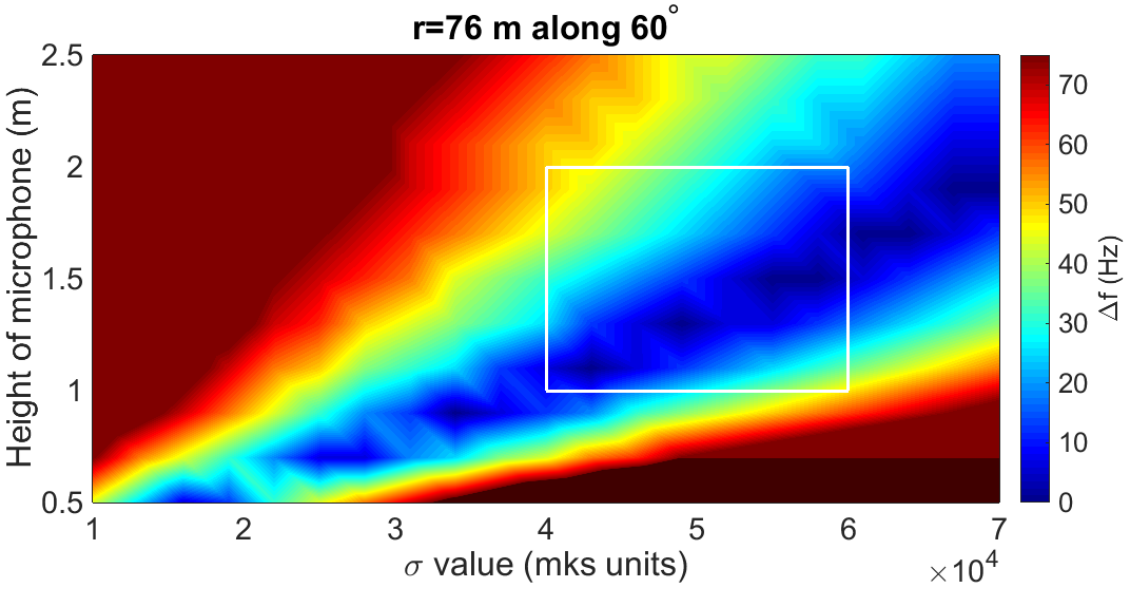

Figure 8 Sensitivity analysis of mic located at 76 m along 60 degree radial

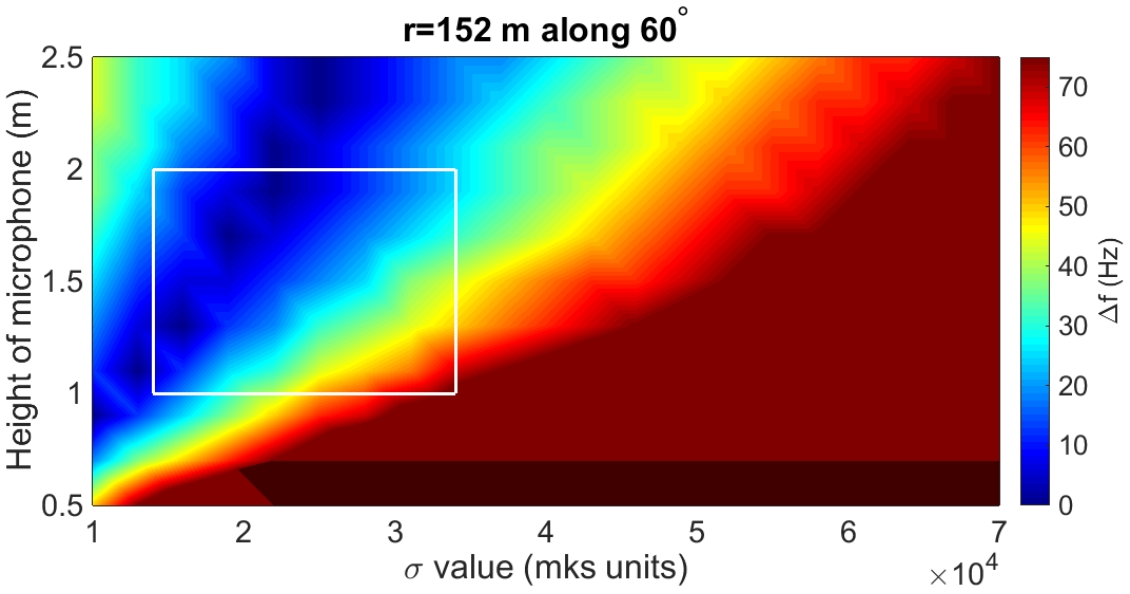

Figure 9 Sensitivity analysis of mic located at 152 m along 60 degree radial

Figure 9 shows the sensitivity analysis plot for the microphone located 152 m along the 60 degree radial. This particular mic shows better agreement with the data at higher microphone heights and at lower sigma values. Lower sigma values indicate a softer or spongier ground[3]; this could indicate greater snow depth between the source and the microphone at 152 m than between the source and the microphone at 76 m. Figure 3 shows the rough, boulder-strewn plain where the data was collected. A possible explanation for why the data from this mic differed so much from the data collected by the other two microphones along the 60 degree radial is sound scattering from rough terrain features.

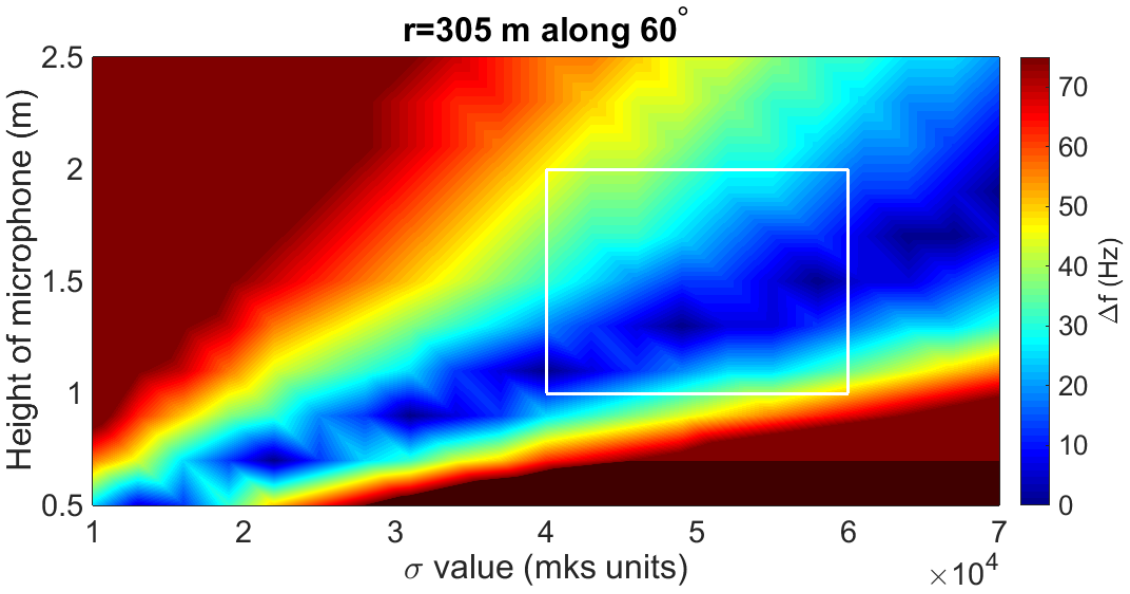

Figure 10 Sensitivity analysis of mic located at 305 m along the 60 degree radial

Figure 10 displays the sensitivity analysis plot of a mic located 305 m along the 60 degree radial. It agrees more closely with Figure 8. At a microphone height 1-2 m high relative to the ground beneath the origin, an effective sigma value between forty and sixty thousand rayls best correlates with the GEM-60 null. The agreement between this plot and Figure 8 leads me to believe that something was awry with the microphone used to collect data at 152 m along the sixty degree radial.

Despite the apparent discrepancy between Figure 9 and Figure 10, the range of sigma values predicted by the ground reflection model agrees with the literature.

3.4 Conclusions

The goal of this study was to perform a sensitivity analysis to discover the parameters to which the effects of ground reflection were most sensitive. The main conclusion is that the frequency of the reflection null in data collected from a horizontal rocket motor test fire is most sensitive to microphone height and to the effective flow resistivity of the ground.

The methods outlined in this paper provide a way to measure the suitability of the parameters selected for a ground reflection model. This paper was limited to analyzing the data set collected on February 19, 2009. A similar analysis could be performed on other data sets collected June 24, 2008 or Sept 6, 2012, and will likely yield higher values of effective flow resistivity due to the lack of snow cover. These results can be used to analyze the values selected for the geometries and flow resistivities in the paper titled: "Including source correlation and atmospheric turbulence in a ground reflection model for rocket noise."[1]

Appendix A

This section describes research performed during the summer of 2014. Section A.1 describes measurements taken using ANSI Standard S1.18-1999[8]. This standard has since been updated, and follow-up work may be necessary to update the codes and methods described in this section to reflect the more current standard. In Section A.2, my work with various computational methods for calculating the numerical distance[3] is described.

Summer Research 2014

A.1 ANSI Standard S1.18-1999

This standard describes a method for obtaining the ground impedance using acoustic methods. In general, a source and two receivers are positioned in one of three set geometric configurations, as in Figure 11, with the receivers positioned at the same distance from the receiver, but at two different heights. Geometry A, for example, has a receiver located on the left, a horizontal range of 1.75 m from the two receivers. The top and bottom receivers are located at heights of 46 cm and 23 cm, respectively, as measured from the ground. The standard assumes a flat, level surface. The standard provides a method for obtaining the best

A subsection of this standard, called Annex A, lists a detailed example of how to obtain the effective flow resistivity from a number of measurements using a given geometry. Following the process described in the standard, I coded AnnexA.m to verify the results reported in Annex A. This code finds a value for the function EE (given in Equation [11]) that gives the best fit. The lowest value of EE should give the sigma value that best characterizes the ground. The value given in AnnexA.m was found by inputting the values from Table A.1 and performing the operations described in Equations [8]-[11] to find the best sigma value. The value returned by

AnnexA.m agrees with the value reported in the standard; however, it should be noted that this code finds a value of 16.7 for a sigma value of $320x10^3$ rayls, and the standard reports a value of 16.

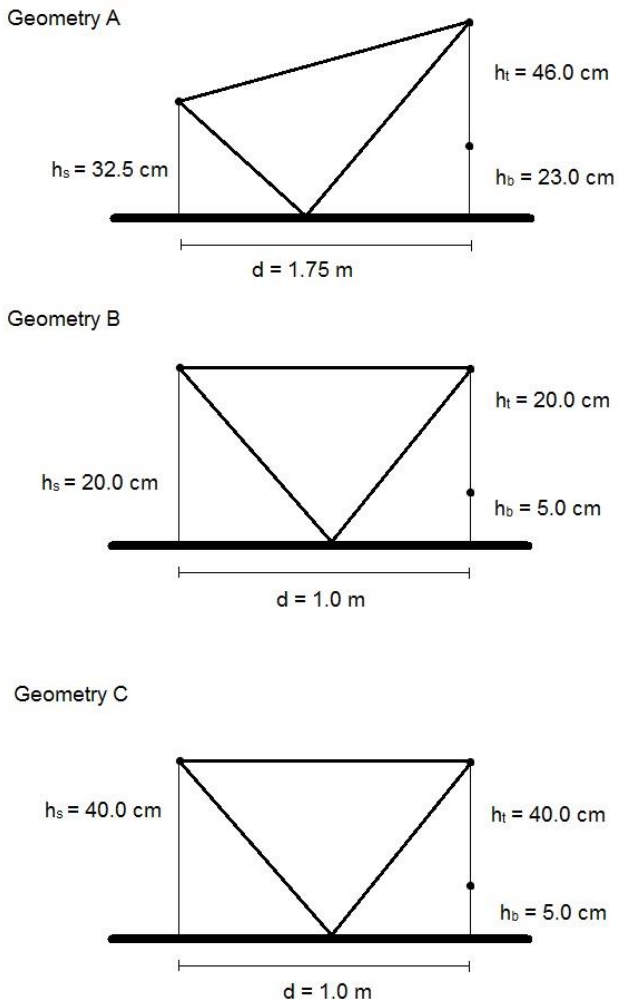

Figure 11 Set geometries for source-receiver configuration, as given in ANSI S1.18-1999

A.2 Analyzing Recent Measurements

Using the code thus developed, I created a program to analyze data taken at various places around campus and at the Bonneville Salt Flats. The program ARG_Impedance_Test.m

calls on a function called levelDifference.m. The function levelDifference.m accepts a sigma value, geometry (A, B, or C as shown in Figure 11), and temperature; it returns the difference in sound pressure level between the two microphones used. This allows you to quickly iterate through a range of sigma values to find the best sigma value using Equation [11] of the ANSI Standard. When measuring the ground impedance above a grassy area, there was some uncertainty in the exactness of the measurements of the microphone height. I created the MATLAB function levelDifferenceHi.m to create an easy way to add measurement errors.

Updates have been made to the ANSI Standard[13] used in these programs. Future work may be necessary to update these files to reflect the methods and techniques of the revised standard.

A.3 Work with the Fadeeva Function

The real and imaginary parts of the numerical distance formulas given by Chessel[14] and Embleton[3] depend on the Fadeeva function. I looked into different computational methods of handling the numerical distance *W*, which is commonly calculated using some old FORTRAN code known as the Fadeeva function. After reading several papers, I coded up several equations found in the literature[3,6,14]. The code fadeeva_test.m plots the real and imaginary parts of the required distance formulas[3,15].

Appendix B

MATLAB Codes

ARG_Impedance_Test.m

```
clear all;
% Ground reflection code that uses Embleton JASA 1983 as a reference
geo='A'; % Specific geometries (A,B, or C) as proscribed in the standard ANSI
S1.18-1999
temp=33.3; % temperature (degrees C)
kk=1;
for sigma=0e6:10e6:100e6%[1e3:10e3:110e3 25e5] %[40 200 300 600 1000 1500
8000];%1e3:5e4:2000000%[600 670 1000]%[670 1060 42.7e3]
    Lc=levelDifferenceHi(sigma,geo,temp);
%%
set(0,'DefaultFigurePosition',[100          100        1000         400]);
set(0,'DefaultAxesLineWidth',2);
set(0,'DefaultLineLineWidth',2);
set(0,'DefaultAxesFontSize',20);

pathname='Z:\Students\Samuel Hord\ESM 2014\Impedance Measurements\Concrete A
8-18-14';
testname='ID';  % Root test name from Data Recorder

ii=1;
switch geo
    case 'A'
        ind=2:1:8; % Test Number
%           ind=[2 5];
    case 'B'
%         ind=[8,9,10,13];
        ind=15:1:20;
    case 'C'
        ind=22:1:27;  % Salt Flats
%           ind=22:1:25; % Grass C
end
for ID=ind
    CH0=0;     % Channel Number - Top Mic
    CH1=1;     % Channel Number - Bottom Mic
    fs=50000; % Sampling Frequency (Hz)
    numbins=101; % Number of Histogram bins

    % % Load Filename
    x0=binfileload(pathname,testname,ID,CH0,7.6*fs,1*fs);
    x1=binfileload(pathname,testname,ID,CH1,7.6*fs,1*fs);
    N=length(x0);
    t = linspace(0,(N-1)/fs,N);
    df=5;

%     %     Plot time data
%     figure
%     plot(t,x1)
```

```
%     xlabel('Time (s)')
%     ylabel('Pressure (Pa)');
%     grid on

    ns=fs/5;
    [f,PSD0,OASPL0] = psdcalc(x0,fs,ns,length(x0)); % Calculates PSD
    [f,PSD1,OASPL1] = psdcalc(x1,fs,ns,length(x1)); % Calculates PSD
    SPL0=20*log10(sqrt((PSD0*df))/2e-5);            % Converts PSD to SPL and
subtracts ambient noise
    SPL1=20*log10(sqrt((PSD1*df))/2e-5);            % Converts PSD to SPL and
subtracts ambient noise
    OASPLtd0=OASPLcalc(x0);                         % Calculates OASPL
    OASPLtd1=OASPLcalc(x1);                         % Calculates OASPL

    deltaL(:,ii)=SPL0-SPL1;

% % %     Plot PSD data
% %     figure
% %     semilogx(f,10*log10(PSD1/2e-5^2))%,'g',f,10*log10(PSD4/2e-5^2),'b')
% %     title('Power Spectral Density')
% %     xlabel('Frequency (Hz)');
% %     ylabel('PSD (dB re 20 \muPa/\surdHz)');
% %     legend('Dyson (Operator Position)','Ambient','Location','SW')
% %     axis tight
% %     grid on

%     % % Plot SPL data
%     figure
%     semilogx(f,Lc,'r-');
%     hold on
%     semilogx(f,SPL0-SPL1)
%     title(['Theory with Measured SPL (\sigma=',num2str(sigma,'%g'),'
rayls)'])
%     ylabel('dB re 20 \muPa')
%     xlabel('frequency (Hz)')
%     xlim([100 4000])
% %     axis tight
%     legend('Theory','Measured','Location','SW')
%     grid on

    ii=ii+1;
end

%% Procedure to Determine Best Fit
% % The standard is valid only for frequencies between 250 and 4000 Hz

% % Uncomment to use the 1/3 octave bands as per the example in the standard
% jj=1;
% for ff=[250,315,400,500,630,800,1000,1250,1600,2000,2500,3150,4000]
% ind(jj)=find(f==ff);
% jj=jj+1;
% end

% Finds the indices of the frequencies between 250 and 4000 Hz
ind=find(f>245&f<4005);
```

```
minn=min(ind);
maxx=max(ind);

[m,n]=size(deltaL);
mysum = sum(10.^(deltaL/10),2);
deltaLave=10*log10(1/n.*mysum);
mystd=std(deltaL,0,2);

% for ii=1:1:n
%     %     dev=1/(n-1).*sqrt(sum((deltaL(ind,ii)-deltaLave(ind)).^2,2));
%     dev=1/(n-1).*sqrt(sum((deltaL(ind,ii)-deltaLave(ind)).^2,2));
% end
EE(kk)=sum(((Lc(ind)-deltaLave(ind))./mystd(ind)).^2)
sig(kk)=sigma;
figure
semilogx(f,deltaLave,'b',f,Lc,'r--')
title('Average SPL difference between top and bottom mic')
xlabel('Frequency (Hz)')
ylabel('dB re 20 \muPa')
xlim([100 10000])
legend('Average', 'Calculated difference','Location','NW')
kk=kk+1;
end
%%
figure
plot(sig,EE)
title('EE vs \sigma_e_f_f')
xlabel('\sigma_e_f_f')
ylabel('EE')

mind=find(EE==min(EE));
freud=sig(mind);
fprintf('\nSigma effective of %i minimizes EE\n',freud)
```

function Lc = levelDifference(sig,geo,temp)

```
% This function computes the calculated level difference per ANSI S1.18-1999
% or per Embleton JASA 1983. Uncomment out the Embleton lines to switch
% between the two.

sigma=sig;
Temp=temp; % Temperature in degrees Celsius

switch geo
    case 'A'
        r=1.75;    % Horizontal distance in m (ft * .3048)
        zs=.325;   % Height of source in m (ft * .3048)
        z1=.46;    % Height of top receiver in m (ft * .3048)
        z2=.23;    % Height of bottom receiver in m
    case 'B'
        r=1.;    % Horizontal distance in m (ft * .3048)
        zs=.2;  % Height of source in m (ft * .3048)
        z1=.2;  % Height of top receiver in m (ft * .3048)
        z2=.05; % Height of bottom receiver in m

    case 'C'
        r=1;    % Horizontal distance in m (ft * .3048)
        zs=.4;  % Height of source in m (ft * .3048)
        z1=.4;  % Height of top receiver in m (ft * .3048)
        z2=.05; % Height of bottom receiver in m
end

f=0:5:24995;  % frequency array in Hz
c=331.4+.6*Temp;          % Sound speed in m/s
k=2*pi*f/c;     % Wavenumber
sigma=sigma;     % Flow resistivity in mks units (Upper limit is 1e9)
rho=1.21;       % Density of Air
S=1;            % Source amplitude (used to scale, but code only saves
relative dB anyway)

sigma=sigma/1000;       % change to cgs rayls

% Top Mic
R1_t=sqrt(r^2+(z1-zs)^2);  % direct path length
R2_t=sqrt(r^2+(z1+zs)^2);  % image path length
% theta_top =atan2((zs+z1),r); % angle of incidence per Embleton 1983
theta_top =atan2(r,(zs+z1)); % angle of incidence per ANSI S1.18-1999

% Bottom Mic
R1_b=sqrt(r^2+(z2-zs)^2);  % direct path length
R2_b=sqrt(r^2+(z2+zs)^2);  % image path length
% theta_bot =atan2((zs+z2),r); % angle of incidence per Embleton 1983
theta_bot =atan2(r,(zs+z2)); % angle of incidence per ANSI S1.18-1999

% calculation of impedances and wavenumber in ground

Z1=rho*c;
Z2=Z1.*(1+9.08*(f/sigma).^-.75+i*11.9*(f/sigma).^-.73);
k2=k.*(1+10.8*(f/sigma).^-.7+i*10.3*(f/sigma).^-.59);
```

```
% % Calculation of reflection coefficient and numerical distance

% % Top
% Rp_t=(Z2*sin(theta_top)-Z1*sqrt(1-
k.^2./k2.^2./cos(theta_top).^2))./(Z2*sin(theta_top)+Z1*sqrt(1-
k.^2./k2.^2./cos(theta_top).^2));% Embleton 1983
% d_t=sqrt(i*2*k*R2_t./(1-Rp_t).^2.*(Z1./Z2).^2.*(1-
k.^2/k2.^2*cos(theta_top)^2)); %Embleton 1983
Rp_t=(Z2*cos(theta_top)-Z1)./(Z2*cos(theta_top)+Z1);  % ANSI S1.18-1999
d_t=(1+i)./2*sqrt(k*R2_t).*(Z1./Z2+cos(theta_top)); % ANSI S1.18-1999

% % Bottom
% Rp_b=(Z2*sin(theta_bot)-Z1*sqrt(1-
k.^2./k2.^2./cos(theta_bot).^2))./(Z2*sin(theta_bot)+Z1*sqrt(1-
k.^2./k2.^2./cos(theta_bot).^2)); % Embleton 1983
% d_b=sqrt(i*2*k*R2_b./(1-Rp_b).^2.*(Z1./Z2).^2.*(1-
k.^2/k2.^2*cos(theta_bot)^2)); % Embelton 1983
Rp_b=(Z2*cos(theta_bot)-Z1)./(Z2*cos(theta_bot)+Z1); % ANSI S1.18-1999
d_b=(1+i)./2*sqrt(k*R2_b).*(Z1./Z2+cos(theta_bot)); % ANSI S1.18-1999


% % Calculation of spherical reflection coefficient

%  Top
[serfc,fail]=W(d_t);
F_t=1+i*d_t*sqrt(pi).*serfc;
% Bottom
[serfc2,fail2]=W(d_b);
F_b=1+i*d_b*sqrt(pi).*serfc2;



Q_t=Rp_t+(1-Rp_t).*F_t;  % Inherently assumes near-grazing incidence.  Seems
to work acceptably though.
Q_b=Rp_b+(1-Rp_b).*F_b;  % Inherently assumes near-grazing incidence.  Seems
to work acceptably though.



% Calculation of relative sound pressure level

pc_t=S*(exp(i*k.*R1_t)./R1_t)+Q_t.*S/1.*(exp(i*k.*R2_t)./R2_t);
pcfree_t=S*(exp(i*k.*R1_t)./R1_t);

pc_b=S*(exp(i*k.*R1_b)./R1_b)+Q_b.*S/1.*(exp(i*k.*R2_b)./R2_b);
pcfree_b=S*(exp(i*k.*R1_b)./R1_b);
%pcfree=1;

% % Calculated level difference
% deltaLc=20*log10(abs(pc_t./pcfree_t))-20*log10(abs(pc_b./pcfree_b)); % per
Embleton
% deltaLc=deltaLc'; % per Embleton
```

```
Lp_t=10*log10(1+(R1_t/R2_t)^2.*abs(Q_t).^2+2*R1_t/R2_t.*abs(Q_t).*cos(k*(R2_t
-R1_t)+atan2(imag(Q_t),real(Q_t)))); % ANSI S1.18-1999
Lp_b=10*log10(1+(R1_b/R2_b)^2.*abs(Q_b).^2+2*R1_b/R2_b.*abs(Q_b).*cos(k*(R2_b
-R1_b)+atan2(imag(Q_b),real(Q_b)))); % ANSI S1.18-1999
deltaLp=Lp_t-Lp_b; % ANSI S1.18-1999
Lc=deltaLp';
```

function Lc = levelDifferenceHi(sig,geo,temp)

```
% This function computes the calculated level difference per ANSI S1.18-1999
% or per Embleton JASA 1983. Uncomment out the Embleton lines to switch
% between the two.

sigma=sig;
Temp=temp; % Temperature in degrees Celsius

% If you know the approximate error in the distance measurements, you can
% add it here.
er1=0;   %.0254/2;
er2=-.01;%-.0254*1.3571;%er1;
er3=0;   %.0254*.0357;%er1/2;
er4=+.01;
switch geo
    case 'A'
        r=1.75+er1;    % Horizontal distance in m (ft * .3048) with a little
uncertainty in position
        zs=.325+er2;   % Height of source in m (ft * .3048)
        z1=.46+er3;    % Height of top receiver in m (ft * .3048)
        z2=.23+er4;    % Height of bottom receiver in m
    case 'B'
        r=1+er1;    % Horizontal distance in m (ft * .3048) with a little
uncertainty in position
        zs=.2+er2;  % Height of source in m (ft * .3048)
        z1=.2+er3;  % Height of top receiver in m (ft * .3048)
        z2=.05+er4; % Height of bottom receiver in m

    case 'C'
        r=1+er1;    % Horizontal distance in m (ft * .3048) with a little
uncertainty in position
        zs=.4+er2;  % Height of source in m (ft * .3048)
        z1=.4+er3;  % Height of top receiver in m (ft * .3048)
        z2=.05+er4; % Height of bottom receiver in m
end

f=0:5:24995;  % frequency array in Hz
c=331.4+.6*Temp;          % Sound speed in m/s
k=2*pi*f/c;     % Wavenumber
sigma=sigma;%*1e3     % Flow resistivity in mks units (Upper limit is 1e9)
rho=1.21;       % Density of Air
S=1;            % Source amplitude (used to scale, but code only saves
relative dB anyway)

% sigma=sigma/1000;       % change to cgs rayls

% Top Mic
R1_t=sqrt(r^2+(z1-zs)^2);  % direct path length
R2_t=sqrt(r^2+(z1+zs)^2);  % image path length
% theta_top =atan2((zs+z1),r); % angle of incidence per Embleton 1983
theta_top =atan2(r,(zs+z1)); % angle of incidence per ANSI S1.18-1999

% Bottom Mic
R1_b=sqrt(r^2+(z2-zs)^2);  % direct path length
R2_b=sqrt(r^2+(z2+zs)^2);  % image path length
```

```
% theta_bot =atan2((zs+z2),r); % angle of incidence per Embleton 1983
theta_bot =atan2(r,(zs+z2)); % angle of incidence per ANSI S1.18-1999

% calculation of impedances and wavenumber in ground

Z1=rho*c;
Z2=Z1.*(1+9.08*(f/sigma).^-.75+i*11.9*(f/sigma).^-.73);
k2=k.*(1+10.8*(f/sigma).^-.7+i*10.3*(f/sigma).^-.59);


% % Calculation of reflection coefficient and numerical distance

% % Top
% Rp_t=(Z2*sin(theta_top)-Z1*sqrt(1-
k.^2./k2.^2./cos(theta_top).^2))./(Z2*sin(theta_top)+Z1*sqrt(1-
k.^2./k2.^2./cos(theta_top).^2));% Embleton 1983
% d_t=sqrt(i*2*k*R2_t./(1-Rp_t).^2.*(Z1./Z2).^2.*(1-
k.^2/k2.^2*cos(theta_top)^2)); %Embleton 1983
Rp_t=(Z2*cos(theta_top)-Z1)./(Z2*cos(theta_top)+Z1);  % ANSI S1.18-1999
d_t=(1+i)./2*sqrt(k*R2_t).*(Z1./Z2+cos(theta_top)); % ANSI S1.18-1999

% % Bottom
% Rp_b=(Z2*sin(theta_bot)-Z1*sqrt(1-
k.^2./k2.^2./cos(theta_bot).^2))./(Z2*sin(theta_bot)+Z1*sqrt(1-
k.^2./k2.^2./cos(theta_bot).^2)); % Embleton 1983
% d_b=sqrt(i*2*k*R2_b./(1-Rp_b).^2.*(Z1./Z2).^2.*(1-
k.^2/k2.^2*cos(theta_bot)^2)); % Embelton 1983
Rp_b=(Z2*cos(theta_bot)-Z1)./(Z2*cos(theta_bot)+Z1); % ANSI S1.18-1999
d_b=(1+i)./2*sqrt(k*R2_b).*(Z1./Z2+cos(theta_bot)); % ANSI S1.18-1999


% % Calculation of spherical reflection coefficient

%  Top
[serfc,fail]=W(d_t);
F_t=1+i*d_t*sqrt(pi).*serfc;
% Bottom
[serfc2,fail2]=W(d_b);
F_b=1+i*d_b*sqrt(pi).*serfc2;



Q_t=Rp_t+(1-Rp_t).*F_t;  % Inherently assumes near-grazing incidence.  Seems
to work acceptably though.
Q_b=Rp_b+(1-Rp_b).*F_b;  % Inherently assumes near-grazing incidence.  Seems
to work acceptably though.



% Calculation of relative sound pressure level

pc_t=S*(exp(i*k.*R1_t)./R1_t)+Q_t.*S/1.*(exp(i*k.*R2_t)./R2_t);
pcfree_t=S*(exp(i*k.*R1_t)./R1_t);
```

```
pc_b=S*(exp(i*k.*R1_b)./R1_b)+Q_b.*S/1.*(exp(i*k.*R2_b)./R2_b);
pcfree_b=S*(exp(i*k.*R1_b)./R1_b);
%pcfree=1;

% % Calculated level difference
% deltaLc=20*log10(abs(pc_t./pcfree_t))-20*log10(abs(pc_b./pcfree_b)); % per
Embleton
% deltaLc=deltaLc'; % per Embleton

Lp_t=10*log10(1+(R1_t/R2_t)^2.*abs(Q_t).^2+2*R1_t/R2_t.*abs(Q_t).*cos(k*(R2_t
-R1_t)+atan2(imag(Q_t),real(Q_t)))); % ANSI S1.18-1999
Lp_b=10*log10(1+(R1_b/R2_b)^2.*abs(Q_b).^2+2*R1_b/R2_b.*abs(Q_b).*cos(k*(R2_b
-R1_b)+atan2(imag(Q_b),real(Q_b)))); % ANSI S1.18-1999
deltaLp=Lp_t-Lp_b; % ANSI S1.18-1999
Lc=deltaLp';
```

Fadeeva_test.m

```
clear;
n=1;
% For reasonaby small values of w (|w|<10):
for w=0:.1:10
    F_w_Chessell(n)=1+i*exp(-w)*(pi*w)^.5-2*w*exp(-
w)*(1+w/(factorial(1)*3)+w^2/(factorial(2)*5) ...
        +w^3/(factorial(3)*7)+w^4/(factorial(4)*9)+w^5/(factorial(5)*11));

    F_w_Embleton(n)=1+i*(pi*w)^.5*exp(-w)*erfc(sqrt(w));
    n=n+1;
end
figure
plot(0:.1:10,F_w_Chessell,'rx',0:.1:10,F_w_Embleton,'bo')
title('For reasonaby small values of w (|w|<10)')
xlabel('w')
ylabel('Fadeeva Function')
legend('Chessell','Embleton')

clear;
n=1;
for w=10:.1:100
    F_w_Chessell(n)=-
(1/2*w+1*3/(2*w)^2+1*3*5/(2*w)^3+1*3*5*7/(2*w)^4+1*3*5*7*9/(2*w)^5);

    F_w_Embleton(n)=1+i*(pi*w)^.5*exp(-w)*erfc(sqrt(w));
    n=n+1;
end
figure
plot(10:.1:100,F_w_Chessell,'rx',10:.1:100,F_w_Embleton,'bo')
title('For larger values of w (|w|>10)')
xlabel('w')
ylabel('Fadeeva Function')
legend('Chessell','Embleton')

%% Chessell- Ingard and Rudnick approximations
clear;
NN=1000;  % Number of frequencies between 1 and 10^5 to investigate
c1=343;  % Speed of sound in 1st medium
c2=1500; % Speed of sound in 2nd medium
p01=1.21;
p02=1026;
siggma=30e6; %arbitrary value chosen...

Z1=415;
Z2=1.54*10^6; % p0*c (Salt water-arbitrary choice)

r1=8; %See FIG. 1 of the Chessell paper (arbitrary geometry chosen)
r2=5; %See FIG. 1 of the Chessell paper

phi=atan(3/4);
phi1=phi;
```

```
% Ingard's Rp
I_Rp=(sin(phi1)-Z1/Z2)/(sin(phi1)+Z1/Z2);

n=1;
for f=logspace(0,5,NN)
    k1=2*pi*f/c1;
    k2=2*pi*f/c2;

    % These are for the computation of the exact value (Embleton 1983)
    R2=p01*c1*(1+9.08*(f/siggma)^-.75);
    X2=p01*c1*11.9*(f/siggma)^-.73;
    E_Z2=R2+i*X2; % Z2=R2+i*beta_2
    betta2=k1*(10.3*(f/siggma)^-.59);
    alphha2=k1*(1+10.8*(f/siggma)^-.70);
    E_k2=alphha2+i*betta2;

    %Rudnick's Rp
    R_Rp=(sin(phi1)-Z1/Z2*(1-(k1/k2)^2*cos(phi)^2)^.5)/(sin(phi1)...
        +Z1/Z2*(1-(k1/k2)^2*cos(phi)^2)^.5);

    %Embleton's Rp (same as Rudnick's)
    E_Rp=(sin(phi1)-Z1/E_Z2*(1-(k1/E_k2)^2*cos(phi)^2)^.5)/(sin(phi1)...
        +Z1/E_Z2*(1-(k1/E_k2)^2*cos(phi)^2)^.5);

    % w(n)
    R_w(n)=2*i*k1*r2/((1-R_Rp)^2*(cos(phi))^2)*(Z1/Z2)^2*(1-
k1^2*(cos(phi))^2/...
        k2^2);

    I_w(n)=1/2*i*k1*r2*(sin(phi)+Z1/Z2)^2/(1+sin(phi)*Z1/Z2);

    E_w(n)=2*i*k1*r2/((1-E_Rp)^2)*(Z1/E_Z2)^2*(1-k1^2*(cos(phi))^2/E_k2^2);

    if abs(R_w(n))<10
        R_F_w_Chessell(n)=1+i*exp(-R_w(n))*(pi*R_w(n))^.5-2*R_w(n)*exp(-
R_w(n))*...

(1+R_w(n)/(1*3)+R_w(n)^2/(factorial(2)*5)+R_w(n)^3/(factorial(3)*7)+...
            R_w(n)^4/(factorial(4)*9)+R_w(n)^5/(factorial(5)*11));
    else
        R_F_w_Chessell(n)=-
(1/2*R_w(n)+1*3/(2*R_w(n)).^2+1*3*5/(2*R_w(n)).^3+1*3*5*7/(2*R_w(n)).^4+...
            1*3*5*7*9/(2*R_w(n)).^5);
    end
    if abs(I_w(n))<10
        I_F_w_Chessell(n)=1+i*exp(-I_w(n))*(pi*I_w(n))^.5-2*I_w(n)*exp(-
I_w(n))*...

(1+I_w(n)/(1*3)+I_w(n)^2/(factorial(2)*5)+I_w(n)^3/(factorial(3)*7)+...
            I_w(n)^4/(factorial(4)*9)+I_w(n)^5/(factorial(5)*11));
    else
        I_F_w_Chessell(n)=-
(1/2*I_w(n)+1*3/(2*I_w(n)).^2+1*3*5/(2*I_w(n)).^3+1*3*5*7/(2*I_w(n)).^4+...
            1*3*5*7*9/(2*I_w(n)).^5);
    end
```

```
    F_w_Embleton(n)=W(sqrt(E_w(n)));
    F_w_Embleton(n)=1+i*(pi*E_w(n))^.5*F_w_Embleton(n);

    n=n+1;
end
f=logspace(0,5,NN);
figure
plot(f,real(R_F_w_Chessell),'b-.',f,real(I_F_w_Chessell),'r:',f,
real(F_w_Embleton),'g--')
title('Real F(w)')
% axis([0 10^5 -10 10])
xlabel('frequency')
ylabel('F(w)')
legend('Real Chessell-Rudnick','Real Chessell-Ingard','Real
Embleton','Location','SW')

figure
plot(abs(R_w),real(R_F_w_Chessell),'b-
.',abs(I_w),real(I_F_w_Chessell),'r:',abs(E_w), real(F_w_Embleton),'g--')
title('Real F(w)')
% axis([0 10^5 -10 10])
xlabel('Abs(w)')
ylabel('F(w)')
legend('Real Chessell-Rudnick','Real Chessell-Ingard','Real
Embleton','Location','SW')

figure
plot(real(R_w),real(R_F_w_Chessell),'b-
.',real(I_w),real(I_F_w_Chessell),'r:',real(E_w), real(F_w_Embleton),'g--')
title('Real F(w)')
% axis([0 10^5 -10 10])
xlabel('Real(w)')
ylabel('F(w)')
legend('Real Chessell-Rudnick','Real Chessell-Ingard','Real
Embleton','Location','SW')

figure
plot(imag(R_w),real(R_F_w_Chessell),'b-
.',imag(I_w),real(I_F_w_Chessell),'r:',imag(E_w), real(F_w_Embleton),'g--')
title('Imag F(w)')
% axis([0 10^5 -10 10])
xlabel('Imag(w)')
ylabel('F(w)')
legend('Real Chessell-Rudnick','Real Chessell-Ingard','Real
Embleton','Location','SW')

figure
plot(f,imag(R_F_w_Chessell),'b',f,imag(I_F_w_Chessell),'r:',f,
imag(F_w_Embleton),'g--')
title('Imaginary F(w)')
% axis([0 10^5 -10 10])
xlabel('frequency')
ylabel('F(w)')
legend('Imaginary Chessell-Rudnick','Imaginary Chessell-Ingard','Imaginary
Embleton')
```

```
figure
plot(real(R_w),imag(R_F_w_Chessell),'b',real(I_w),imag(I_F_w_Chessell),'r:',r
eal(E_w), imag(F_w_Embleton),'g--')
title('Imaginary F(w)')
% axis([0 10^5 -10 10])
xlabel('Real(w)')
ylabel('F(w)')
legend('Imaginary Chessell-Rudnick','Imaginary Chessell-Ingard','Imaginary
Embleton')

figure
plot(imag(R_w),imag(R_F_w_Chessell),'b',imag(I_w),imag(I_F_w_Chessell),'r:',i
mag(E_w), imag(F_w_Embleton),'g--')
title('Imaginary F(w)')
% axis([0 10^5 -10 10])
xlabel('Imag(w)')
ylabel('F(w)')
legend('Imaginary Chessell-Rudnick','Imaginary Chessell-Ingard','Imaginary
Embleton')

figure
plot(abs(R_w),imag(R_F_w_Chessell),'b',abs(I_w),imag(I_F_w_Chessell),'r:',abs
(E_w), imag(F_w_Embleton),'g--')
title('Imaginary F(w)')
% axis([0 10^5 -10 10])
xlabel('w')
ylabel('F(w)')
legend('Imaginary Chessell-Rudnick','Imaginary Chessell-Ingard','Imaginary
Embleton')

%
% %% Also, the Ground Absorption Model (Chessell 1977)
% clear;
% NN=10000;  % Number of frequencies between 1 and 10^5 to investigate
% c0=343;  % Speed of sound in 1st medium
% p0=1.21;
%
% m=1;
% for siggma=[100,200,300]
%     n=1;
%     for f=[50,100,200,500,1000,2000,5000,10000]
%
%         R(n)=(1+9.08*(f/siggma)^-.75);
%         X(n)=(11.9*(f/siggma)^-.73);
%         Alpha(n)=(1+10.8*(f/siggma)^-.70);
%         Beta(n)=10.3*(f/siggma)^-.59;
%
%         Z(n)=R(n)+i*X(n);
%         k(n)=Alpha(n)+i*Beta(n);
%
%         zphase(n)=atan(X(n)/R(n));
%         kphase(n)=atan(Beta(n)/Alpha(n));
%
%         ff(n)=f;
%
```

```
%         n=n+1;
%     end
%
%
%     subplot(4,1,1)
%     semilogx(ff,abs(Z))
%     title('FIG. 2 Chessell Paper')
% %     xlabel('FREQUENCY - Hz')
%     ylabel('MAGNITUDE - Z')
%     hold on
%
%     subplot(4,1,2)
%     semilogx(ff,zphase)
% %     xlabel('FREQUENCY - Hz')
%     ylabel('Phase - Rad.')
%     hold on
%
%     subplot(4,1,3)
%     semilogx(ff,abs(k))
% %     xlabel('FREQUENCY - Hz')
%     ylabel('MAGNITUDE - k')
%     hold on
%
%     subplot(4,1,4)
%     semilogx(ff,kphase)
%     xlabel('FREQUENCY - Hz')
%     ylabel('Phase - Rad.')
%     hold on
%
%     m=m+1;
% end
% hold off
% % %%
% % clear;
% % f=logspace(0,5,24)
```

Works Cited

[1] Gee, Kent L., Tracianne B. Neilsen, and Michael M. James. "Including source correlation and atmospheric turbulence in a ground reflection model for rocket noise." *168th Meeting of the Acoustical Society of America* (Indianapolis, IN, October 2014). Proceedings of Meetings on Acoustics **22** , 040001 (2014).

[2] Attenborough, Keith. "Propagation of Sound above a Porous Half-space." The Journal of the Acoustical Society of America **68** (1980): 1493.

[3] Embleton, T. F. W. "Effective Flow Resistivity of Ground Surfaces Determined by Acoustical Measurements." The Journal of the Acoustical Society of America **74** (1983): 1239.

[4] Delany, M.e., and E.n. Bazley. "Acoustical Properties of Fibrous Absorbent Materials." Applied Acoustics **3** (1970): 105-16.

[5] Kinsler, Lawrence E., Austin R. Frey, Alan B. Coppens, and James V. Sanders. Fundamentals of Acoustics. New York: J. Wiley, 2000. Print.

[6] Daigle, G. A. "Effects of Atmospheric Turbulence on the Interference of Sound Waves near a Fintite Impedance Boundary." The Journal of the Acoustical Society of America **64** (1978): 622.

[7] Daigle, G. A. "Effects of Atmospheric Turbulence on the Interference of Sound Waves above a Finite Impedance Boundary." The Journal of the Acoustical Society of America **65** (1979): 45.

[8] ANSI S1.18-1999. "Template Method for Ground Impedance." (2004).

[9] Muhlestein, Michael B., Kent L. Gee, Derek C. Thomas, and Tracianne B. Neilsen. "Prediction of Nonlinear Propagation of Noise from a Solid Rocket Motor." *The Journal of the Acoustical Society of America* **132** (2012): 1992.

[10] Gee, Kent L., Jarom H. Giraud[†], Jonathan D. Blotter, and Scott D. Sommerfeldt. "Energy-Based Acoustical Measurements of Rocket Noise." 1*5th AIAA/CEAS Aeroacoustics Conference (30th AIAA Aeroacoustics Conference)*, (May 2009, Miami, FL), AIAA Paper 2009-3165.

[11] Gee, Kent L., R. Jeremy Kenny, Tracianne B. Neilsen, Trevor W. Jerome[†], Christopher M. Hobbs, and Michael M. James. "Spectral and statistical analysis of noise from reusable solid rocket motors." Proceedings of Meetings on Acoustics **18**, 040002 (2013).

[12] "Graphite-Epoxy Motor." Wikipedia. Wikimedia Foundation, n.d. Web. 14 Apr. 2015.

[13] ANSI S1.18-2010. " Method for Determining the Acoustic Impedance of Ground Surfaces." (2010).

[14] Chessell, C. I. "Propagation of Noise along a Finite Impedance Boundary." The Journal of the Acoustical Society of America 62.4 (1977): 825.